

Atmospheric heat redistribution and collapse on tidally locked rocky planets

Robin Wilder

School of Engineering and Applied Sciences, Harvard University

Cambridge, MA 02138, USA

Received _____; accepted _____

ABSTRACT

Abstract text describing the study's findings. The text is heavily garbled and contains many nonsensical characters and words, making it largely illegible. It appears to discuss a 3D general circulation model (GCM) and its results, but the specific details are obscured by the noise.

k

₂ and CO). For

1. Introduction

Introduction text describing the background and objectives of the study. The text is heavily garbled and contains many nonsensical characters and words, making it largely illegible. It appears to discuss the importance of the study and its goals, but the specific details are obscured by the noise.

eight or a decade (Meyer et al 2009; Chabaud et al 2009; Pepin et al 2011; Tintin et al 2012), and the dedicated solar wind mission Parker Solar Probe (PSP) is expected to provide the first in-situ measurements of the solar wind at the inner edge of the heliosphere (Borini et al 2010; Chabaud et al 2011; DePaul et al 2012; Kieffer et al 2013; Fainberg et al 2014). However, the solar wind is a complex and dynamic plasma that is not yet fully understood (Sckelton et al 2011; Carrasco et al 2011; Mihalov et al 2011; Sauer et al 2014).

Because of the large number of solar wind ions, the solar wind is a multi-species plasma. The solar wind is composed of several ion species, including protons, alpha particles, and various heavy ions (e.g., Fe, Si, Mg, Ca, Ni, S, O, C, N, Ne, Ar, Kr, Xe). The solar wind is also a multi-temperature plasma, with different ion species having different temperatures. The solar wind is a collisionless plasma, meaning that the mean free path of the ions is much larger than the size of the solar system. This makes the solar wind a unique and challenging environment for studying plasma physics. The solar wind is also a source of space weather, which can affect the Earth's magnetosphere and cause geomagnetic storms. The solar wind is a key component of the heliosphere, and understanding its properties is essential for understanding the solar system and the interstellar medium.

The solar wind is a multi-species plasma, and the different ion species have different properties. The solar wind is also a multi-temperature plasma, and the different ion species have different temperatures. The solar wind is a collisionless plasma, and the different ion species have different collisionless lengths. The solar wind is also a source of space weather, and the different ion species have different effects on the Earth's magnetosphere.

¹We do not define the term 'Eak' here, although it is commonly used in the literature to refer to the Earth's magnetosphere.

Earth's atmosphere is a complex system that has been the subject of extensive research. The study of the atmosphere is crucial for understanding climate change and the impact of human activities. This paper discusses the current state of atmospheric science and the challenges ahead.

The atmosphere is a thin layer of gases surrounding the Earth. It is composed of various gases, including nitrogen, oxygen, and carbon dioxide. The atmosphere plays a vital role in regulating the Earth's temperature and protecting life from harmful solar radiation.

The atmosphere is a dynamic system that is constantly changing. It is influenced by natural processes such as volcanic eruptions and human activities such as the burning of fossil fuels. Understanding the atmosphere is essential for predicting future climate conditions.

Earth's energy balance is a key concept in atmospheric science. It refers to the balance between the energy received from the Sun and the energy lost to space. This balance is crucial for maintaining the Earth's temperature.

The greenhouse effect is a natural process that warms the Earth's surface. It occurs when greenhouse gases in the atmosphere trap heat from the Sun. This process is essential for life on Earth.

The atmosphere is a complex system that is constantly changing. It is influenced by natural processes such as volcanic eruptions and human activities such as the burning of fossil fuels. Understanding the atmosphere is essential for predicting future climate conditions.

The atmosphere is a complex system that is constantly changing. It is influenced by natural processes such as volcanic eruptions and human activities such as the burning of fossil fuels. Understanding the atmosphere is essential for predicting future climate conditions.

The atmosphere is a complex system that is constantly changing. It is influenced by natural processes such as volcanic eruptions and human activities such as the burning of fossil fuels. Understanding the atmosphere is essential for predicting future climate conditions.

A comprehensive understanding of the atmosphere is essential for predicting future climate conditions. This requires a combination of observational data and climate models. The atmosphere is a complex system that is constantly changing. It is influenced by natural processes such as volcanic eruptions and human activities such as the burning of fossil fuels. Understanding the atmosphere is essential for predicting future climate conditions.

Numerous studies have been conducted to better understand the atmosphere. These studies have shown that human activities are a major driver of climate change. The atmosphere is a complex system that is constantly changing. It is influenced by natural processes such as volcanic eruptions and human activities such as the burning of fossil fuels. Understanding the atmosphere is essential for predicting future climate conditions.

etal (2013)]. The ~~fresh~~ ~~edited~~ ~~second~~ ~~and~~ ~~the~~ ~~press~~
~~htae~~ ~~kybe~~ ~~pnih~~ ~~tlay~~ ~~okd~~ ~~egin~~ ~~How~~ ~~to~~ ~~hm~~
~~foad~~ ~~apshl~~ ~~barface~~ ~~ps~~ ~~ad~~ ~~Eak~~ ~~ch~~
~~to~~ ~~h~~ ~~cent~~ ~~sible~~ ~~debyad~~ ~~apir~~ ~~is~~ ~~he~~ ~~sofican~~
~~in~~ ~~at~~ ~~Eak~~ ~~spost~~ ~~ps~~ ~~Eak~~ ~~ap~~ ~~(coea)~~ ~~in~~
~~geal~~ ~~Here~~ ~~is~~ ~~ly~~ ~~a~~ ~~derage~~ ~~to~~ ~~sen~~ ~~is~~ ~~ce~~ ~~sy~~

². Becau

Underly ~~ap~~ ~~hated~~ ~~stad~~ ~~ch~~ ~~sp~~ ~~ch~~ ~~upn~~
~~in~~ ~~co~~ ~~to~~ ~~fu~~ ~~pcal~~ ~~bs~~ ~~nd~~ ~~ok~~ ~~ps~~ ~~This~~ ~~bf~~ ~~fo~~
~~ng~~ ~~ps~~ ~~ad~~ ~~pol~~ ~~fo~~ ~~ng~~ ~~cas~~ ~~ps~~ ~~ca~~ ~~fu~~ ~~car~~ ~~be~~
~~deid~~ (Setal 2011). ~~Ge~~ ~~n~~ ~~ch~~ ~~if~~ ~~de~~ ~~GCM~~ ~~s~~ ~~er~~ ~~po~~ ~~n~~
~~ide~~ ~~g~~ ~~accu~~ ~~cy~~ ~~the~~ ~~ba~~ ~~nced~~ ~~by~~ ~~ad~~ ~~ves~~ ~~ib~~ ~~is~~ ~~of~~ ~~g~~ ~~l~~ ~~fo~~ ~~ta~~
~~bs~~ ~~is~~ ~~to~~ ~~be~~ ~~an~~ ~~d~~.

Here a ~~ge~~ ~~al~~ ~~ly~~ ~~ap~~ ~~is~~ ~~by~~ ~~fo~~ ~~l~~ ~~ay~~ ~~okd~~ ~~ps~~ ~~ad~~ ~~M~~ ~~s~~
~~sc~~ ~~o~~ ~~o~~ ~~d~~ ~~e~~ ~~d~~ ~~fu~~ ~~g~~ ~~as~~ ~~GCM~~ ~~h~~ ~~is~~ ~~ad~~ ~~to~~ ~~ly~~ ~~per~~ ~~fo~~
~~hated~~ ~~bu~~ ~~fo~~ ~~l~~ ~~ay~~ ~~o~~ ~~g~~ ~~is~~ ~~le~~ ~~It~~ ~~is~~ ~~th~~ ~~in~~ ~~pa~~ ~~yn~~ ~~o~~
~~to~~ ~~ng~~ ~~pa~~ ~~yn~~ ~~ps~~ ~~h~~ ~~g~~ ~~le~~ ~~face~~ ~~ep~~ ~~ta~~ ~~can~~
~~be~~ ~~ed~~ ~~an~~ ~~al~~ ~~ly~~ ~~be~~ ~~ca~~ ~~pp~~ ~~er~~ ~~de~~ ~~id~~ ~~fo~~ ~~r~~ ~~GCM~~
~~is~~ ~~Ne~~ ~~x~~ ~~t~~ ~~h~~ ~~GCM~~ ~~is~~ ~~in~~ ~~had~~ ~~co~~ ~~o~~ ~~l~~ ~~e~~ ~~d~~ ~~-~~

k ~~de~~ ~~ad~~ ~~ad~~ ~~to~~ ~~ly~~

~~ch~~ ~~ps~~ ~~aca~~ ~~age~~ ~~to~~ ~~bar~~ ~~fl~~ ~~is~~ ~~ap~~ ~~is~~ ~~ps~~ ~~ad~~ ~~pa~~ ~~yn~~ ~~as~~ ~~We~~
~~fo~~ ~~so~~ ~~p~~ ~~CO~~ ₂ ~~ch~~ ~~to~~ ~~as~~ ~~ty~~ ~~ca~~ ~~se~~ ~~be~~ ~~CO~~ ~~is~~ ~~ch~~ ~~de~~ ~~ig~~
~~gas~~ ~~The~~ ~~gas~~ ~~se~~ ~~ch~~ ~~beca~~ ~~us~~ ~~hy~~ ~~ae~~ ~~co~~ ~~l~~ ~~u~~ ~~s~~ ~~to~~ ~~ba~~ ~~in~~ ~~g~~ ~~as~~

²RecehWag ad Read (2012) ad Kajad Sim(2014) ad a GCM tin
~~he~~ ~~ch~~ ~~ges~~ ~~ir~~ ~~ch~~ ~~fo~~ ~~ra~~ ~~age~~ ~~to~~ ~~pa~~ ~~nc~~ ~~is~~ ~~o~~ ~~ll~~ ~~g~~ ~~face~~ ~~ps~~ ~~How~~
~~by~~ ~~fo~~ ~~sd~~ ~~ch~~ ~~est~~ ~~is~~ ~~it~~ ~~av~~ ~~age~~ ~~h~~ ~~ip~~ ~~er~~ ~~h~~ ~~ae~~ ~~ch~~
~~es~~ ~~ta~~ ~~be~~ ~~ta~~ ~~pi~~ ~~ch~~ ~~ps~~ ~~h~~ ~~ch~~ ~~cas~~ ~~sw~~ ~~ty~~ ~~be~~.

consistently better than the other models. In the
 case of the H_2O and CH_4 bands, the difference between
 the two models is significant. In addition, the
 difference between the two models is significant for
 the CO_2 band. The difference between the two
 models is significant for the CO_2 band.

In Sect. 2, we describe the 3D model. In Sect. 3, we
 describe the 1D model. Next, we describe the
 results of the GCM simulations. Finally, we
 describe the results of the 1D model. The
 results of the 1D model are shown in Fig. 1.
 The results of the 1D model are shown in Fig. 1.
 The results of the 1D model are shown in Fig. 1.

2. Method

For the 3D GCM, we use the LMD GCM model [e.g., Wehr
 et al. (2011); Wehr et al. (2013); Lecoeur et al. (2013)]. The
 results of the GCM are shown in Table 1. The LMD
 model is used to simulate the atmosphere of Mars.

³CO₂, H₂O and O₂, and the ratio CO/O₂ are
 presented in the paper by Masarik and Veys (2006).
 The behavior of O₂ and N₂ is not modeled, but
 the gas is assumed to be well mixed (Fleury
 et al. 2006).

(Gdyad Yg 1989; Wdktetal 2010a). Highh abplaa fo

ph cohd- k delaspued g h pnc fuc

kspectrum

ad h HITRAN h dabas (Rbmetal 2009; Rbmetal 2010). CO

2

chued abpsidled g h GBB pncin(Wdkt

etal 2010a; Ga ad Bpl998; Bauretal 2004), hexpif h

daa ad atepmsabo 400 K. Imcassh face gajasad b

be flat Allive pfoa gna g-cpulealgasap,

hapi cdesteped asinWdktetal (2011). FrCO, h

appa cu ascpd g a ChhChpulealgasahw

paecderid folide (2000). Sface h hataup(du te.g., h

psne f ameah) isahgectd. Bpfcam chtrak h pem

macabé, bthysaba caw p rinh ctalchp

pa ⁴. Uh inWdktetal (2011), cd adat fog isahgectd.

Th h effectsb cd ad aeadat fog ae disad iSect4. Th

face abedo A isahbe 0.2, a epsh ah fropst Frh M-ar

ps idlg h shpctnda foAD Leo(Ges 388) isad, asin

psies(Segna etal 2003; Wdktetal 2010b). AD Leoahact in

h XUV ad degosfoflag eos(Shetal 2009), bth ps

docmhbe aswae foad ndat pessih trape.

Rayhshatg isidled asinWdktetal (2010a), ah effectsae

hd ad M-asbecas f hred-hed pca. Th pnyb isad

⁴Negctg ndeg backd gasscaw p hbecas pa

bndeg f abpsneassa ah pnc fuc btad M-

ssneassih ad Rayhshatg hve h effectopnyabedo

[e.g., Wdktetal (2010b); aPaletal (2010).]

characteristic time scale Ω is given by the Keplerian orbital period Ω_K scaled by the ratio of the stellar radius R_* to the orbital distance a :

$$\Omega = \frac{2\pi}{1 \text{ year}} \left(\frac{M}{M_\odot} \right)^{1/2} \left(\frac{L}{L_\odot} \right)^{-3/4} \left(\frac{F}{F_E} \right)^{3/4} \quad (1)$$

Here M , L and F are the stellar mass, luminosity and flux, respectively. For the Sun, $M = M_\odot$, $L = L_\odot$ and $F_E = 1361 \text{ W m}^{-2}$ (Peters and Chan 1981; Rein et al 2009), (1) can be written as

$$\Omega = 9.2 \times 10^{-9} F^{3/4}. \quad (2)$$

Here we have used $F_E = 2732 \text{ W m}^{-2}$ and a value of $\Omega = 2 \times 10^{-8} \text{ s}^{-1}$ for the characteristic time scale. This is a reasonable value for the characteristic time scale of the tidal forcing. The tidal forcing is assumed to be constant over the lifetime of the star.

For the protoplanetary disk (PBL), the migration is assumed to be in the regime of Type I migration (Mebad Yanda 1982), which is characterized by a migration rate that is proportional to the surface density of the disk (1988) and the migration rate is independent of the disk mass (Habel et al 1993; Fogli et al 1999), which is the case considered here. In brief, the Mebad Yanda / Gap (MYG) migration is a steady-state migration that is driven by the tidal torque exerted by the protoplanet on the disk. The migration rate is given by $\dot{a} = -\frac{2}{3} \frac{a}{\tau} \frac{\partial \Theta}{\partial z}$, where τ is the migration timescale, Θ is the tidal torque, and z is the vertical coordinate. The migration rate is independent of the disk mass and the migration rate is given by $\dot{a} = -\frac{2}{3} \frac{a}{\tau} \frac{\partial \Theta}{\partial z}$.

Yamada 1982). The above is applicable for epifaunal law
 of Backlund (1962)

$$l = \frac{l_0 \mathcal{K} z}{\mathcal{K} z + l_0} \quad (3)$$

where $\mathcal{K} = 0.4$ is a constant and l_0 is a constant length
 in boundary

The exchange coefficient is called free surface velocity
 The vertical diff. coefficient
 are called as

$$\left. \frac{\partial \mathbf{u}}{\partial t} \right|_{turb} = \frac{\partial}{\partial z} \left(K_M \frac{\partial \mathbf{u}}{\partial z} \right) \quad (4)$$

$$\left. \frac{\partial \Theta}{\partial t} \right|_{turb} = \frac{\partial}{\partial z} \left(K_H \frac{\partial \Theta}{\partial z} \right) \quad (5)$$

given t , at high z , the vector $\mathbf{u} = (u, v)$, the
 Θ and eddy and diff. coefficients K_M and K_H . Diff. coefficient
 are called by M. O'Brien (Gant 1994) is q , l and h gradient

Richardson number is defined as the ratio of energy in
 flow

$$Ri = \frac{g}{\Theta} \frac{\partial \Theta}{\partial z} \left[\left(\frac{\partial u}{\partial z} \right)^2 + \left(\frac{\partial v}{\partial z} \right)^2 \right]. \quad (6)$$

Index for Richardson number can be defined as

$$Ri_B = \frac{g \Delta \Theta / \Theta}{|\mathbf{u}|^2 / \Delta z}, \quad (7)$$

where Δz is height from face and $\Delta \Theta$ is potential difference
 between face and a particular level

At a face, the exchange is called as

$$\mathcal{F}(f) = C_D \rho_a |\mathbf{u}| (f_a - f_s) \quad (8)$$

be \mathcal{F} is the flux of f , C_D is the drag coefficient, ρ_a and $|\mathbf{u}|$ are the air density and wind speed, respectively. f_a and f_s are the surface and subsurface fluxes, respectively, for $f = |\mathbf{u}|$, $f_s = 0$. The drag coefficient is defined as

$$C_D = \left(\frac{\mathcal{K}}{\ln[z/z_0]} \right)^2 \quad (9)$$

where z_0 is the roughness length, z_0 is the surface roughness parameter, which can be found in the literature (e.g., (Dyer 1975; Head et al 1985; Roth et al 2011)). Here we adopt the values for z_0 from Table 1. Note that the dependence of C_D on z_0 is weak in the range of z_0 values considered here (Wesely et al 2011).

3. Results

3.1. Idealised 3D GCM simulations

To begin with, we consider idealised 3D GCM simulations of a planet with a surface pressure of 0.01, 0.1 and 1 bar. The gas is assumed to be composed of CO_2 . Earth is assumed to have $r_p = r_E$, $g = g_E$ and $F = F_E = 1366 \text{ W m}^{-2}$ are assumed. When the atmosphere is assumed to be composed of CO_2 , the mean molecular weight is $\bar{m} = 44 \text{ g mol}^{-1}$.

$$\tau = \frac{\kappa p_s}{g \bar{m} \alpha}, \quad (10)$$

where p_s is the surface pressure, g is the gravity, \bar{m} is the mean molecular weight, $\alpha = 0.5$ is the fraction of molecules in the ground state. We set $\kappa = 5.0 \times 10^{-5} \text{ m}^2/\text{g}$, yielding $\tau = 0.1$ at 0.1 bar.

planetary regime for $h > 3$ in Asche et al. (2013) is
 $L_{Ro} = \frac{R \sqrt{c_p T_e}}{c_p 2\Omega r_p}$

Figure 1 shows the face temperature and its variation
 $p_s = 0.1$ bar. The plot shows a large temperature
difference and a sharp peak at the pole, which is
discussed in the text. To a first order approximation
the effect is to increase the temperature based
on a simple model of a rotating planet.

⁵ the

$$\frac{L_{Ro}}{r_p} = \sqrt{\frac{R \sqrt{c_p T_e}}{c_p 2\Omega r_p}} \quad (11)$$

is 2.06, which is a typical value for the effect of the
rotation (Lecath et al. 2013). In (11),

R and c_p are the specific gas constant

and specific heat capacity (for CO₂)

r_p is the planetary radius

$T_e = [(1 - A)F/4\sigma]^{1/4}$ is the global equilibrium

Figure 2 (left) shows the face temperature at equilibrium
for different values. The dashed line shows the temperature
at the pole (back) in 0.01 and 0.1 bar cases, which is
at 1 bar. This indicates that the temperature at the pole
is a factor of 10-100 higher than the average
temperature.

⁵ Note that the definition of L_{Ro} used here is
 $L_{Ro} = \frac{R \sqrt{c_p T_e}}{c_p 2\Omega r_p}$ and, in the literature, L_{Ro} can be defined by
 $L_{Ro} = \frac{R \sqrt{c_p T_e}}{c_p 2\Omega r_p}$ (Lecath et al. (2013) definition)
or $L_{Ro} = \frac{R \sqrt{c_p T_e}}{c_p 2\Omega r_p}$.

$L_{Ro} = (\sqrt{gH_s}/\beta)^{1/2}$ or $L_{Ro} = (\sqrt{NH_s}/N)$

Fig 2 (g) is a day and night averaged vertical profile in the high Albedo surface region. The aspect ratio is $Ri_B = 2^{1/4} T_e$ at the surface, depending on the surface temperature, day and night differences in day and night. The general feature is that the temperature is higher in the day than at night [e.g., (Mead and Schuler 2010; Pierrehet 2011b)], which is typical for a WTG regime (Sbeletal 2001). The surface temperature is $p_s = 0.1$ bar. The surface temperature is $T_{as\Theta} = T(p_s/p)^{R/c_p}$, where p and p_s are the surface and sea level pressure.

$$T_{skin} = 2^{1/4} T_e \text{ at}$$

The general feature is that the temperature is higher in the day than at night. Fig 4 is a plot of the surface fluxes and the surface temperature as a function of the surface pressure. The surface fluxes are shown in the range of 0.01 and 0.1 bar. The surface temperature is also shown as a function of the surface pressure. The surface fluxes are shown in the range of 0.01 and 0.1 bar. The surface temperature is also shown as a function of the surface pressure. The surface fluxes are shown in the range of 0.01 and 0.1 bar. The surface temperature is also shown as a function of the surface pressure.

The behavior of the surface fluxes and the surface temperature is shown in Fig 4. The surface fluxes are shown in the range of 0.01 and 0.1 bar. The surface temperature is also shown as a function of the surface pressure. The surface fluxes are shown in the range of 0.01 and 0.1 bar. The surface temperature is also shown as a function of the surface pressure.

$$Ri_B \text{ is defined as}$$

and the drag coefficient (5-8) are large, leading to efficient mixing in the surface.

The double-paked structure becomes a flat face in particular
in detail.

On the other hand, the significant created by the point in
the boundary. The use of the English oak
age-sab cich Mig is the ad a side hatflux
cylinders. A fair (agbse) and by the
the. The, ad a c g tpe does face hatbdget a
payday becomes a hard edge ad a angle of
a side hatflux is a (Ceraid Pakl 1984).

Fig 5 (p) is a managed face in ped θ_z in the
of the change. The data in Fig 5 is derived by a 2D face
of the fields $|u| = \sqrt{u^2 + v^2}$ from GCM to the
a sharp ad a g. All the pakatad $\theta_z = 40^\circ$, by
is at 0.01 ad 0.1 barad a reduced pakil ped in 1 barcas. The
of the ped each is a sharp dip in the hatflux
is (Fig. 4) ad the a sharp face point in 1 barcas. For
0.01 ad 0.1 barcas, a side hatflux is a due a day
face points

The 0.1 bar $|u| \propto \theta_z$ ad p (b) is a jet (p60 m $^{-1}$)
in the air. This is a half a flow in the face in
Fig. 1; a in ped in a $p_s/2$ indicates a between
flow in the sharp. The air is a point in the
age-sab cich is a for a ge point out cel (se Fig. 6 for
a side). In the sharp face in ped can be a
by a g any

It is a type of a 1 bar $\tau = 1$ (left) to the
 Jetal (1997) type of a 1 bar. The, or day/night differences
 are in the range of 260-270 K, compared to 240 K
 in the Jetal (1997) type of a 1 bar. The
 efficiency of the Jetal (1997) model is a parameter
 based on the data from (Jetal 1995), which
 represents the efficiency of energy transfer between the
 surface and the atmosphere. The
 model is based on the heat flux parameterized
 in the Jetal (1997) Sect. 4.

3.2. Analytical model

The depth of the GCM cell, as described in this
 paper, is a parameter of the model, which is
 a parameter of the model. The
 temperature T_n is a parameter of the GCM-deep coefficient

To illustrate the model, a set of parameters is
 given in Fig. 6. In Fig. 3, which is a
 schematic of the model, the heat flux
 and energy exchange between the surface and the
 atmosphere can be seen. On the other hand, Pechet
 (2011b) and Yagci and Abbott (2014), except for
 the adiabatic GCM model

Given the complexity of the model, it is
 in fact a parameter of the model, a balance of energy

in

$$\sigma T_s^4 = (1 - A)S(\psi, \lambda) + GLR + C_D c_p \rho_a |\mathbf{u}| (T_a - T_s). \quad (12)$$

Here $S(\psi, \lambda) = F \cos \theta_z$ is the solar flux, ψ , λ and θ_z are the, latitude and longitude, respectively. GLR is the ground radiative flux and T_a is the surface air temperature. Since there is no absorption of radiation by the atmosphere, the energy balance can be written as

$$OAR + GLR = \mathcal{A} \sigma T_s^4 + \mathcal{D} + C_D c_p \rho_a |\mathbf{u}| (T_s - T_a) \quad (13)$$

where OAR is the ground radiative flux, \mathcal{A} is the area of the surface, \mathcal{D} is the convective heat flux, $f = c_p T$ is the convective heat flux, and σT_s^4 is the outgoing longwave radiation. The term f in (13) is the convective heat flux, which is given by

Next we define

$$B_d = \frac{\int_d \sigma T_s^4 dA}{2\pi r_p^2} \quad (14)$$

$$B_n = \frac{\int_n \sigma T_s^4 dA}{2\pi r_p^2} \quad (15)$$

where $\int_d dA$ and $\int_n dA$ are the integrals over the day and night, respectively. Using (12) and (13) we can write

$$B_d = \frac{1}{2}(1 - A)F + GLR + C_D c_p \rho_a \overline{|\mathbf{u}| (T_a - T_d)} \quad (16)$$

$$B_n = GLR + C_D c_p \rho_a \overline{|\mathbf{u}| (T_a - T_n)} \quad (17)$$

and

$$OAR + GLR = \frac{1}{2} \mathcal{A} B_d + \frac{1}{2} \mathcal{A} B_n + \frac{1}{2} C_D c_p \rho_a \overline{|\mathbf{u}| (T_d - T_a)} + \frac{1}{2} C_D c_p \rho_a \overline{|\mathbf{u}| (T_n - T_a)} \quad (18)$$

be T_d and T_n are \bar{OAR} and \bar{GLR} respectively

Not because of balance balance and balance

where \bar{OAR} [e.g., $\bar{OAR} = (4\pi r_p^2)^{-1} \int_{\Sigma} OAR dA = OAR$]. We define by

balance \bar{u} and T_d , by being \bar{u} and T_d

balance

If \bar{u} and T_d are the path

$$A \approx \tau \text{ and } \bar{OAR} \approx \bar{GLR} \approx \tau B_a$$

(Péchet2011a). Then (16-18) can be fixed to

$$B_d = \frac{1}{2}(1 - A)F + \tau B_a + C_D c_p \rho_a \bar{u} (T_a - T_d) \quad (19)$$

$$B_n = \tau B_a + C_D c_p \rho_a \bar{u} (T_a - T_n) \quad (20)$$

$$4B_a = B_d + B_n + C_D c_p \rho_a \bar{u} [(T_d - T_a) + (T_n - T_a)]/\tau \quad (21)$$

3.3. Purely radiative case

Five main physical processes are

$$C_D \rightarrow 0 \text{ and } \bar{u}$$

and face-are energy exchange is \bar{u} . Remaining path

equation (19-21) reduce to

$$B_d = \frac{1}{2}(1 - A)F + \tau B_a \quad (22)$$

$$B_n = \tau B_a \quad (23)$$

$$4B_a = B_d + B_n \quad (24)$$

Here

$$B_n = \frac{\tau}{2 - \tau} \frac{(1 - A)F}{4}. \quad (25)$$

Because we already and

$\tau < 1$, can be written as

$$B_n \approx \frac{\tau(1 - A)F}{8}. \quad (26)$$

Here $\bar{\alpha}$ is defined by (10) in $\bar{\alpha} = 0.5$,

$$T_n \approx \left(\frac{(1-A)F\kappa p_s}{4\sigma g} \right)^{1/4}. \tag{27}$$

In the case of a thin radiating layer, the temperature of the layer is given by (27) and can be derived by neglecting a) the back-radiation from the day side and b) the back-radiation from the night side. In this case, the day side temperature is affected by the incoming solar radiation, and the night side temperature is affected by the radiation received from the day side.

Using (27) for the ideal GCM case considered in Sect. 3.1, we get $T_n = 70.4, 125.2$ and 222.7 K for $p = 0.01, 0.1$ and 1 bar, respectively. These values are in good agreement with the GCM [see Fig. 2 (left)], which is in good agreement with the results of the 1D model. However, the results of the 1D model are in good agreement with the results of the GCM. We therefore refer to (27) as the *thin radiator temperature*.

3.4. Inclusion of the dayside sensible heat flux

Now we include the dayside sensible heat flux in the energy balance (19-21). However, a simple analytical solution is not possible for a general case. Specifically, we have to take into account the fluxes of the day side and night side (see Fig. 4) and derive (20) and (21). We also

$B_n \ll B_a$ and $\tau B_a \ll \frac{1}{2}(1 - A)F$. Hence (19-21) become

$$B_d \approx \frac{1}{2}(1 - A)F \tag{28}$$

$$B_n \approx \tau B_a \tag{29}$$

$$4B_a \approx B_d + C_{Dg}c_p \overline{|\mathbf{u}|(T_d/T_a - 1)}/(2\kappa R). \tag{30}$$

For an ideal gas and (10) has been used. We write $\overline{|\mathbf{u}|(T_d/T_a - 1)}$ as

$\chi \overline{|\mathbf{u}|(T_d/T_a - 1)}$, where $|\mathbf{u}|$, T_d and T_a are taken to be independent of χ

is a fact that accounts for the fact that $\theta_z = 0$, whereas $|\mathbf{u}|$ peaks

at 40° . To be self-consistent $T_d/T_a \propto \cos \theta_z$ and $|\mathbf{u}| \propto \sin \theta_z$,

yielding $\chi = \int_0^{\pi/2} \cos^2 \theta_z \sin \theta_z d\theta_z = 1/3$. By defining a dimensionless

parameter $\tilde{T} = T_a/T_d$ and velocity $\tilde{U} = |\mathbf{u}|/U_0$, we

$$U_0 = (1 - A)F \frac{\kappa R}{\chi C_{Dg} c_p} \tag{31}$$

we can write (30) as

$$4\tilde{T}^4 - 1 = \tilde{U}(\tilde{T}^{-1} - 1). \tag{32}$$

(32) defines T_a (and hence T_n) as a function of T_d and $|\mathbf{u}|$ in

3.5. An equation for $|\mathbf{u}|$

To obtain (32), we used a WTG approach. WTG is valid for

convective boundary layer flows (see e.g. Ekanem et al. 2001) and

accelerated flows (see e.g. Beck and Smith 2013), given that

the advection is not too strong. None of these conditions are

met in the present case, but it is

not clear how this affects the

The boundary condition (Vak2006)

$$\frac{DI}{Dt} + \frac{p}{\rho} \nabla \cdot \mathbf{u} = \mathcal{H} \quad (33)$$

where I is the energy per unit mass, p is the pressure, ρ is the density, \mathbf{u} is the velocity, D/Dt is the material derivative and \mathcal{H} is the diabatic heating rate in W/kg, maybe fixed in WTG, ideal gas law

$$\nabla \cdot \mathbf{u} = \frac{1}{RT_a} \mathcal{H}. \quad (34)$$

The essence of (34) is that absence of buoyancy advection effects implies

a fluid with a large density contrast is cooled by the flow

of a neutral atmosphere

\mathcal{H} is the effective radiative heating

and is given by the first term in the balance equation

for the energy budget, $\mathcal{H}_{rad,s}$ and T_a is the ambient temperature. $\mathcal{H}_{rad,s}$ is given by

the energy balance equation, T_a is the ambient temperature

$$\frac{U_1}{L} \sim \frac{1}{RT_d} \mathcal{H}_{rad,s} \quad (35)$$

and hence

$$U_1 \sim \frac{L\kappa(1-A)F}{2RT_d}. \quad (36)$$

L is the characteristic length scale, κ is the absorption coefficient

r_p . The characteristic height U_1 is related to U_0 by defining a density scale height

$H_d = RT_d/g$, where g is the gravity

$$U_1 \sim \frac{r_p (1-A)F\kappa}{H_d 2g} \quad (37)$$

$$U_1 \sim \tilde{L}U_0 \quad (38)$$

where \tilde{L} is the scale height

$$\tilde{L} = \frac{\chi C_D r_p c_p}{2H_d R}. \quad (39)$$

Given $\chi = 1$, $C_D = 0.0034$, $r_p = 10^{-2}$ m and $H_d = 10$ m, $\tilde{L} = 2.4$. We

assume $C_D = 0.0034$. From Earth's atmosphere, $\tilde{L} = 2.4$. We

also that \tilde{L} is a function of \tilde{u} and \tilde{T} and hence of the surface flux from the face.

Next, from (34), we have $\nabla \cdot \mathbf{u} \sim |\mathbf{u}|/r_p$, and the divergence is

$$\frac{|\mathbf{u}|}{r_p} = \frac{1}{RT_a} \left(\kappa\sigma T_d^4 - 2\kappa\sigma T_a^4 + \frac{g\chi C_D |\mathbf{u}| c_p (T_d - T_a)}{RT_a} \right) \quad (40)$$

The final term in the surface flux is a small correction to the divergence, divided by a factor p_s/g together with the pressure gradient. Using (40) and (34) can be used to create an explicit expression

$$\tilde{U} = \frac{\tilde{L}(1 - 2\tilde{T}^4)}{\tilde{T} + 2\tilde{L}(1 - \tilde{T}^{-1})}. \quad (41)$$

Substituting (41) into (32) we get

$$(4\tilde{T}^4 - 1) [\tilde{T} + 2\tilde{L}(1 - \tilde{T}^{-1})] - \tilde{L}(1 - 2\tilde{T}^4)(\tilde{T}^{-1} - 1) = 0. \quad (42)$$

The parameters \tilde{T} and \tilde{L} can be determined by using the values of \tilde{T} and \tilde{U} as shown in Fig. 7. Given $\tilde{L} = 2.4$, we find $\tilde{U} = 6.2$ and $\tilde{T} = 0.85$. For $U_0 = 1.2 \text{ m s}^{-1}$, $|\mathbf{u}| = 7.4 \text{ m s}^{-1}$, which is close to the value in Fig. 5.

Fig. 8 shows the face temperature predicted by (29) given the surface gas exchange GCM from the face of Ascarbe and the complete set of parameters, in (29) given the GCM and T_n . The ‘radiation’ (20) depends on the GCM and the surface temperature and can be expressed by factoring the surface temperature. A simple expression for the surface flux is also possible, and we address it in

3.6. Multiband 3D GCM simulations

High depth a priori studies of the features of the
 atmospheric gas and the weather of the
 planet GCM model - k and k after Fig. 9. The
 a priori study of 0.1 bar GCM model parameters
 as in Fig. 3. The model - k and k after Fig. 9. The
 CO (and ν_2) band is the most effective in the
 at 0.1 bar. As can be seen in Fig. 10, the
 model is generally of CO and ν_2 band, the
 the model is the best model.

The efficiency of the CO band can be determined by
 the model of the CO ν_2 and CO (Fig. 10). As can be seen in
 bands of CO ν_2 are the most important in the
 the CO band is the most important in the
 model. The model is the best model.
 the model, and the model is the best model.
 calculated at ν_2 band is the most important
 centered at 2143.27 cm^{-1} (Godyad Yu 1989). CO ν_2 ,
 due to lack of a priori study of the
 667 cm^{-1} ($15 \mu\text{m}$) and 2325 cm^{-1} ($4.3 \mu\text{m}$) bands
 of the model. The model is the best model.
 generally, the model is the best model.
 preceding study of the model is the best model.
 and the model is the best model.
 In the model, the model is the best model.

concentrations

The atmospheric temperature profile (Fig. 10; grey) is primarily determined by radiative cooling of CO₂ and H₂O in the atmosphere. The atmospheric temperature profile is shown in Fig. 10 (grey line). The atmospheric temperature profile is shown in Fig. 10 (grey line). The atmospheric temperature profile is shown in Fig. 10 (grey line).

When the atmospheric temperature profile is shown in Fig. 10 (grey line), the atmospheric temperature profile is shown in Fig. 10 (grey line). The atmospheric temperature profile is shown in Fig. 10 (grey line).

The atmospheric temperature profile is shown in Fig. 10 (grey line). The atmospheric temperature profile is shown in Fig. 10 (grey line). The atmospheric temperature profile is shown in Fig. 10 (grey line).

As can be seen from the atmospheric temperature profile in Fig. 10 (grey line), the atmospheric temperature profile is shown in Fig. 10 (grey line). The atmospheric temperature profile is shown in Fig. 10 (grey line).

⁶ Although it is a real gas, the atmospheric temperature profile is shown in Fig. 10 (grey line). The atmospheric temperature profile is shown in Fig. 10 (grey line).

the critical shear flow is created according to eqn

$$\log_{10} \left[\frac{p_{crit}}{1 \text{ Pa}} \right] = c_1 F_s^3 + c_2 F_s^2 + c_3 F_s + c_4 \quad (43)$$

where the coefficients c_i are determined by least squares fit. The values are in Fig 11, and the coefficients are in Table 2.

The above observations are general and are not

scale as F_s increases as a result of a given

case. The shear flow is precisely and hence a given

point decreases. In addition, the shear flow is a function

$t_{adv} = r_p / |\mathbf{u}|$ is the shear flow. However, in WTG eqn

say \tilde{U} and \tilde{L} are the shear flow effects. It is

The decrease in critical shear flow can be determined by

reference to (27). The shear flow is a function of the shear

flow, and hence a critical shear flow can be determined before the onset

Because the shear flow is a function of the shear flow, the shear

is affected by the critical shear flow. However, it

is not possible to determine the shear flow as a function of the shear

4. Discussion

The shear flow is a function of the shear flow, and

the shear flow is a function of the shear flow, and

the shear flow is a function of the shear flow, and

the shear flow is a function of the shear flow, and

the shear flow is a function of the shear flow, and

However, the shear flow is a function of the shear flow, and

the fallacy of a perceived elimination of
 has been. The presence of a direct trace gas is a
 the most likely to be considered, by a
 and it is better to be able to put a
 can be by increased by a surface of the
 as a result of a significant, as well as
 for CO₂ in water (2011), although the
 can find it in the air (Yag et al 2013). For
 the end of the day, the effects of
 the education of the people can be regarded as
 a very high

20

Article is a study of the
 a significant region of the world
 and the results of the study
 are greater than 60% (Sag and Fendó 2001; M
 Gabriel 2007). The effect of the
 here, is to be found in MYG
 significant results.

Shelton (2005) developed a
 at a significant level in the
 gap between the two
 as a result of the
 eddy diffusion, and the
 eddy diffusion, and the
 [Fig. 8 in Shelton (2005)]. At

Ri region is a

Ri near the

at 1 bar, even in a 0.1 bar

CO₂ in a 1 bar atmosphere

Ri_B at the surface is

and 1, in a 1 bar atmosphere

in the troposphere of a GCM

simulation. It is significant that

the gas constant R is

For a diatomic gas, $\gamma = 1.4$

and the effect of the mean free

path length is negligible

in the troposphere of a GCM

simulation. It is significant that

the gas constant R is $R = \frac{8.314}{M}$

where M is the molar mass

$2O$

[e.g., Lecar et al (2013); Menou (2013)],

and the effect of the mean free

path length is negligible

$2, N_2, Ar$

in the troposphere of a GCM

simulation. It is significant that

the gas constant R is

For a diatomic gas, $\gamma = 1.4$

and the effect of the mean free

path length is negligible

in the troposphere of a GCM

simulation. It is significant that

the gas constant R is

had the data. Flyasid et al (2011), for a
subject name, of the paper and
the paper. The general idea is to
find out what is significant

The research by NASA's
VPL team benefited from research by
Peter Read, Bob Haber, Zhi-Kang and Renode K. The
work was supported by FAS Dir Science, Research
Center and University

REFERENCES

- Baker R. V. (2013). The predicted radiative effects of the possible
Monthly Notices of the Royal Astronomical Society,
429(3):20522068.
- Bann Y. I., Laffey W. J., and Fasor G. T. (2004). Infrared spectra of
and absorption of O₂ bands
in O₂/CO₂ mixtures. *J. Mol. Spectrosc.*, 228:432440.
- Bean J. L., Kessler E., and Hoyer D. (2010). A ground-based spectroscopic
survey of Earth's atmosphere. *Nature*, 468:669672.
- Blackadar A. K. (1962). The vertical distribution of humidity in
the atmosphere. *Journal of Geophysical Research*, 67(8):30953102.
- Carr T. and Menon K. (2011). Atmospheric aerosols. *The Astrophysical
Journal Letters*, 743(2):L36.
- Cetin T. A. and Pasha T. R. (1984). A study of the diurnal
variation of humidity. *Journal of Climate and Applied
Meteorology*, 23(11):15631572.
- Chou D., Bell Z. K., Iqbal J., Bell C. J., Nair P., Chou L. A., Liu
C., Bins X., Lam D. W., Udelson S., et al (2009). A prediction of a
nearby star. *Nature*, 462(7275):891894.
- Chou O., Dink J., Ghera A., Gaffo C., Pheger K., Bell J., Riley A., and
Gibson T. (2014). Magnetic field and spin in binary
systems. *arXiv preprint arXiv:1405.7707*.

- Ch B., Abet L., Jayadha, R., KepE. M.-R., FoyJ. J., MnyN.,
ad NehH. (2011). Bondad aspects of h prealgj
1214b ggesa lea bchuwgtape. *The Astrophysical Journal*,
736(2):78.
- DeqB.-O., GhM., Seager S., Beok, B., Dejn D., ad JackB. (2012).
Detectf haleifm preah *The Astrophysical Journal Letters*,
751(2):L28.
- DnG., RechyP., ad GreenR. (1975). Radarmasof anrgap
ad face ps Th 1971 ad 1973 p *Icarus*, 26(3):273312.
- Edn A. R., Kag, J. F., Pnd, D., Lee, S., ad BanP. R. (2012). Th
Cabnt-Stat Cye ad CO2/Ch FeedbackofTidalLock Teral
Phas *Astrobiology*, 12:562571.
- Fget F., Hdin F., Fir R., Hdin C., Tahgad, O., Ch M., Lew
S. R., Read, P. L., ad HnJ. (1999). Inp geal cradlesf
h Mahnape for face tabe 80 kn *Journal of Geophysical
Research*, 104:2415524176.
- Fan, J., Dejn D., Beok, B., KnH., JdanA., Ep, N., Madhan
N., Wk A., ad Tdo K. (2014). Waterapibh clear
ape fa op-e-epet *Nature*, 513(7519):526529.
- Fth L. (2006). *Collision-induced absorption in gases*, kn2. Cabidge
UesPes
- GapB., Kah, L. H., Hail, S., ad Roj A. (1988). A Quisehin
TherEgyMdel forGepalFw *Journal of Atmospheric Sciences*,
45:5562.

- Garin B., Sisk S., and Adams P. S. (2007). On the thermal structure of the atmosphere. *Atmospheric Science Letters*, 8(3):6569.
- Gaut J. R. (1994). *The atmospheric boundary layer*. Cambridge University Press.
- Goody R. M. and Yung, Y. L. (1989). *Atmospheric radiation: theoretical basis, 2nd ed., by Richard M. Goody and YL Yung*. New York, NY: Oxford University Press, 1989, 1.
- Gottlieb M. and Brune A. (1997). Rotational Raman scattering of CO₂ for Venus atmosphere at 250 cm⁻¹, at temperatures 600 to 800 K. *Icarus*, 129:172-177.
- Gottlieb M. and Brune A. (1998). Collisional relaxation of the rotational Raman spectra of CO₂. *Molecular Physics*, 93:1007-1016.
- Haber, R. M., Hansen, H. C., Held, R., and Held, T. (1993). A boundary layer model for the atmosphere of Venus. *Journal of the atmospheric sciences*, 50(11):1544-1559.
- Head, J. W., Pettit, A. R., Garin J. B., and Zisk S. H. (1985). Surface characteristics of Venus from radar and reflection measurements. *Journal of Geophysical Research: Solid Earth (1978-2012)*, 90(B8):6873-6885.
- Heg, K. and Kulkarni, P. (2012). On the Ly α emission from Venus. *The Astrophysical Journal*, 754(1):60.
- Heg, K. and Vignati, S. S. (2011). Geometric albedo of Venus. *Monthly Notices of the Royal Astronomical Society*, 415(3):2145-2157.

- Ige A. P., Sca M. E., and Sch S. G. (1985). Spin obliquity of
Shubert 6. *Icarus*, 64(3):375-390.
- J.M. (2003). The Model Studies of Solar Planets *Astrobiology*,
3:415-427.
- J.M., Ley S., Read, P., and Cah, D. (1995). Westward drift
of the North Atlantic basin. *Journal of
Geophysical Research: Planets (1991-2012)*, 100(E3):5485-5500.
- J.M. M., Haber, R. M., and Reynolds R. T. (1997). Shubert 6
of Solar Type Planets Observed with
Astronomical Habitable *Icarus*, 129:450-465.
- Kay Y. and Sca A. P. (2014). A study of the
age of the planet *arXiv preprint arXiv:1407.6349*.
- Kay, J. F., Williams D. P., and Reynolds R. T. (1993). Habitable
Zone *Icarus*, 101:108-128.
- Khadem M. L., Rbaş I., Lamm H., Gburek J.-M., Lamm M., Sca F.,
Eh, C., Haber A., Ben H. K., Fagn, C. J., et al (2007). Cal
culations of the habitability of
habitable planets in the solar system
and the habitable zone *Astrobiology*, 7(1):167-184.
- Keilberg, L., Bean J., Désj J., Seager S., Dejn D., Beck, B., Bean, Z. K.,
Seager K. B., and Haber D. (2013). The Spectroscopic
Search for GJ 1214b with HST/WFC3 in the
American Astronomical Society Meeting Abstracts, 221.6
American Astronomical Society Meeting Abstracts, page 224.03.

- Lambert H., Lindner H. I. M., Kiselev N., Gebauer J., Tenda, N., Eker N. V., Ben H. K., Khabib M. L., Rbas I., Pen T., and Seb F. (2007). CalMasEjch(CME) Actio LoMasM SasasAnIpn FactoTh Hababif Teris Epos II. CME-Induced InPickUp f Eak EposiCb-InHababe Zas *Astrobiology*, 7:185207.
- Lect, J., Fget F., ChanvB., WdhR., Seb F., ad MbE. (2013). 3d che delg f co-ihd pos Cchupte che in babjad ababy *arXiv preprint arXiv:1303.7079*.
- Lide, D. P., ed(2000). *CRC Handbook of Chemistry and Physics*. CRC PRESS, 81 edh
- LJ. L., Fane, K., ad Ays T. (2013). Cpn LY α flss6 F5 V b M5 V ss *The Astrophysical Journal*, 766(2):69.
- May M., Bfsh X., Fob, T., Defo, X., UdyS., BetuJ., BesH., Boh F., Lis C., Pep, F., Peir C., Qub D., ad SaN. C. (2009). Th HARPS sacifbret-brpos XVIII. AnEahspatih GJ 581 hpaym *Astronomy and Astrophysics*, 507:487494.
- Meb G. L. ad Yanda, T. (1982). Deopt a Thnce Ch Mdelfo GeplaFl Pbesn *Reviews of Geophysics*, 20:851875.
- MenK. (2013). Waerap ds *The Astrophysical Journal*, 774(1):51.
- Mes T. M. ad Schiler T. (2010). Apic dmsf eak ilayokd aqbes *Journal of Advances in Modeling Earth Systems*, 2(4).
- Migu Y., Kabeigger L., FegelyB., ad Schefer L. (2011). Cpf h

- prelates e hrcadilats *The Astrophysical Journal Letters*, 742(2):L19.
- Ma P., Fend H., Pinc, M., Chan W., Kaly T., ad Parly E. (2002). Obsrnf flow hrc in onldayhrcra *Journal of the Atmospheric Sciences*, 59(17):25132534.
- Pep, F., Lis C., Segnan D., Ben W., Bon F., Dep X., May M., Qub D., San N., ad Udy S. (2011). Th hpsachfreak h ps in habbe n: Ieynspsad h20794, h85512 ad h192310. *arXiv preprint arXiv:1108.3447*.
- PezBeck D. ad Sun A. P. (2013). Ape hated btoh *The Astrophysical Journal*, 776(2):134.
- Petn B. R. ad Chan L. A. (1981). Cpe hsrnd daf flae as I - AD Leind GX Adndae. *ApJ*, 251:571582.
- Pechet R. (2011a). *Principles of Planetary Climate*. Cabldge UisPes
- Pechet R. T. (2011b). A pet 6 chesfrGes 581g. *The Astrophysical Journal Letters*, 726(1):L8.
- Reil, N., Reil, I. N., Red, N., ad Haly S. (2000). *New light on dark stars*. Sger
- Reis A., Bai G., ad By, M. (2009). Eileoe fongat flvstih *The Astrophysical Journal*, 692(1):538.
- Rben P., Malden S., Edl M., ad Ry A. (2014). Schracyndg aspsih habbe n 6h ndaf ges 581. *Science*, 345(6195):440444.

- Rohg, M., Ahn O., Head, J., Kesz M., Mazur E., Nem G. A.,
ShD. E., Tene, M. H., ad Zber M. T. (2011). Global face psad
ghsf h dch hberheraber *Journal of Geophysical
Research: Planets (1991–2012)*, 116(E2).
- RhnL., GdnI., Baber R., Dh, H., Ganch, R., GdmA., Peerw
V., TakS., ad TepJ. (2010). Heph htpnt bchr
pscp daabas. *Journal of Quantitative Spectroscopy and Radiative Transfer*,
111(15):21392150.
- RhnL. S., GdnI. E., Babe, A., Benr D. C., BenhP. F., BkM., Bdn
V., BwL. R., Cappa, A., ChpnJ.-P., Choe, K., Cdet L. H.,
Daa, V., Dej V. M., Fay S., Fhd, J.-M., Ganch, R. R., GdmA.,
Jacup D., Kbir I., Laca N., Laffey W. J., MadnJ.-Y., Maie, S. T.,
MhahS. N., Mer C. E., MozaAhdi N., NahnO. V., Nh
A. V., Ohl J., Peerw V. I., PenA., PedicA., Rhd, C. P.,
Rger M., Šick, M., ShM. A. H., Sg, K., TakS. A., Tep
J., ThR. A., Vadaee, A. C., ad VaderAca, J. (2009). Th HITRAN
2008 hchrpscp daabas. *Journal of Quantitative Spectroscopy and
Radiative Transfer*, 110:533572.
- Sadh B., Lecta, J., RahnD., Fgeř F., Léger A., ad Schid J. (2014).
Chg ps cytreash jnwbb tesp. h
cas fcc7b. *arXiv preprint arXiv:1402.6637*.
- Seager S., DnR., etal (2010). *Exoplanets. Uuf Aa Pes*
- Sega, A., Keb, K., Kag, J. F., SahnD., MeadyV., CpD., ChnM.,

- ad Maw E. (2003). On Coenad UhtFlsoEahLk
PhosAd ObrSas *Astrobiology*, 3:689708.
- Ses F., WdrR., ad Fget F. (2011). Thahpe cus6 ng
tealepos I. chaceig apes *Astronomy & Astrophysics*,
532.
- ShE., LiuM. C., ad Reil, I. N. (2009). Idefig h Yg LonsSas
h25 p. I. Spectp Obsarh *ApJ*, 699:649666.
- Sbel A. H., Nhs J., ad Pih L. M. (2001). Th wakentp gadeh
aphad balned palhaws*. *Journal of the atmospheric
sciences*, 58(23):36503665.
- ShC., Gasf O., ad Moqt A. (2007). Masadiscu froahEarh
posad oearpos *Icarus*, 191:337351.
- Sag, E. ad Fendp H. (2001). Vetalgn ad asgha aified
barhgr *Journal of physical oceanography*, 31(8):20262048.
- ShhS., GapiB., ad SashI. (2005). A qalsae ehb
delf hthflsabe aificah *Physics of Fluids (1994-present)*,
17(8):085107.
- TanF. (2009). ThahEsap fospEahApsih Hababè Zasb
M Sas *The Astrophysical Journal*, 703:905909.
- TonM., Jos H. R., Jeh J. S., TiyC. G., Bhr R. P., Vgt S. S., Bas
J. R., Weyn R. A., O'Te, S., Hnr J., etal (2012). Signehcedd in
h adalebja. pic vath h aretobis *arXiv preprint
arXiv:1212.4277*.

- Udry S., Bouché X., Deleaux X., Forveille T., Mayor M., Pepe C., Boch F., Lovis C., Pepe F., Queloz D., and Baran J. (2007). The HARPS search for exoplanets XI. Spectra (5 and 8 M+) in 3-planet systems. *Astron. Astrophys.*, 469:L43-L47.
- Valis G. K. (2006). *Atmospheric and oceanic fluid dynamics: fundamentals and large-scale circulation*. Cambridge University Press
- Wais P., Gebauer S., Grib M., Grefe J. L., Heden P., Kien D., Patz A. B. C., Rauer H., and Sack B. (2010). The exoplanet Gliese 581d: a habitable planet. *Astronomy and Astrophysics*, 522:A23+.
- Wang Y. and Read P. (2012). Direct planetary circulations in the solar system. *Proceedings of the International Astronomical Union*, 8(S293):297-302.
- Ward R., Forget F., and Esposito V. (2010a). Infrared climate and atmospheric CO₂ abundance. *Icarus*, 210:992-997.
- Ward R., Forget F., Michel E., Head J., Maden J.-B., and Chan B. (2013). Global climate on early Mars: Water cycle and ice. *Icarus*, 222(1):149.
- Ward R. and Pierrehumbert R. (2014). Atmospheric CO₂ abundance on early Mars. *The Astrophysical Journal Letters*, 785(2):L20.
- Ward R. D., Forget F., Sels F., Maden J., Michel E., and Esposito V. (2010b). Is Gliese 581d habitable? Spectroscopic constraints. *Astronomy and Astrophysics*, 522:A22+.

Wolfe, R. D., Fegley, F., Seaton, P. G., Miller, E., Chubb, B., and Maden, J.-B.

(2011). *Ge 581d is a Flared Terrestrial Planet*

Habitable Zone. *The Astrophysical Journal Letters*, 733:L48.

Yagci, J. and Abbot, D. S. (2014). *A Habitable Super-Earth*

and a Hot Jupiter

The Astrophysical Journal, 784(2):155.

Yagci, J., Cameron, B., and Abbot, D. S. (2013). *Stable climate*

and habitable zone for a super-Earth

The Astrophysical Journal

Letters, 771(2):L45.

Yung, Y. L. and DeMore, W. B. (1999). *Photochemistry*

of planetary atmospheres/Yung, Y. L., DeMore, W. B. New

York: Oxford University Press, 1999. QB603. A85 Y86 1999, 1.

Table 1: Standard parameters used in the k GCM for Phobos and Deimos. Parameters are taken from (2007) unless otherwise specified.

Parameter	Units	Value
Solar flux	$L [L_{\odot}]$	0.024
Star		AD Leo
Obliquity	e	0.0
Obliquity	ϕ	0.0
Atmospheric pressure	p [bar]	0.01-10.0
Solar flux	F [1366 W/m^2]	0.2-3.0
Planet mass	$M [M_{\oplus}]$	1.0, 10.0
Planet radius	$r [r_{\oplus}]$	1.0, 1.88
Surface gravity	g [m s^{-2}]	9.8, 27.8
Surface roughness	z_0 [m]	1×10^{-2}
Surface albedo	\mathcal{I} [K]	250
Surface albedo	A	0.2
Atmospheric composition	CO	CO_2, CO

Table 2: Coefficients in the polynomial expansion (43).

Planet mass	c_1	c_2	c_3	c_4
$1.0 M_E$	-0.84×10^{-10}	0.73×10^{-6}	-0.0022	6.01
$10.0 M_E$	-0.81×10^{-10}	0.63×10^{-6}	-0.0017	6.34

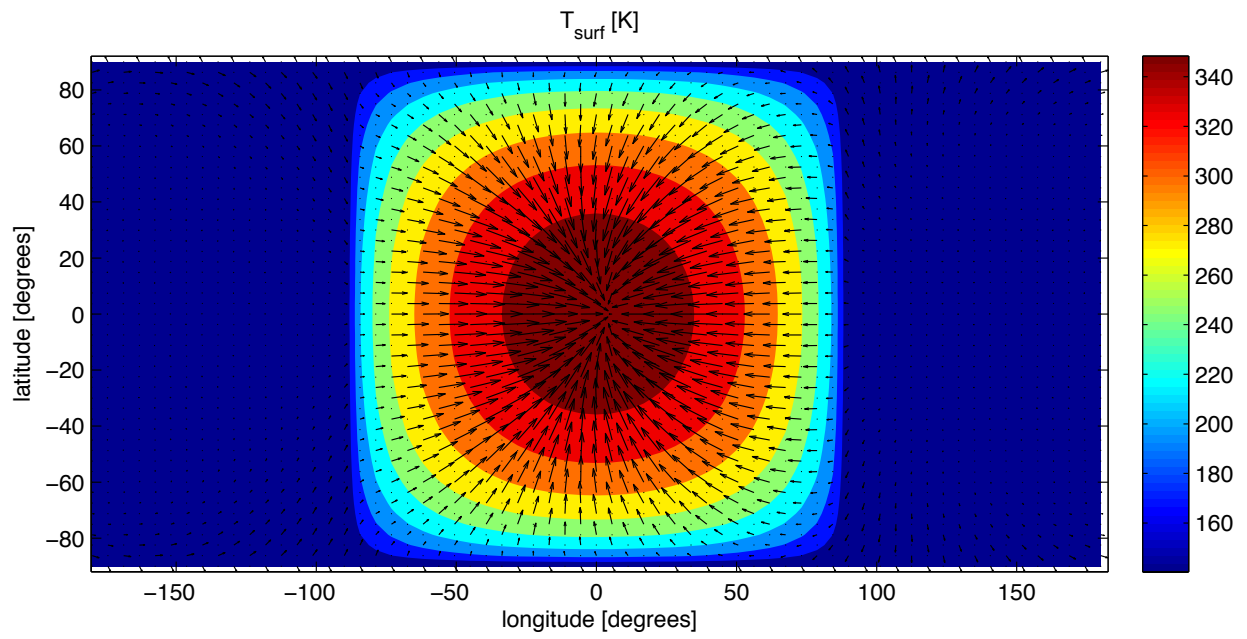


Fig. 1. Temperature map (top) and flow field (bottom) in the 0.1 barg nitrogen atmosphere. The flow field is calculated for the case of a 100 W heat source.

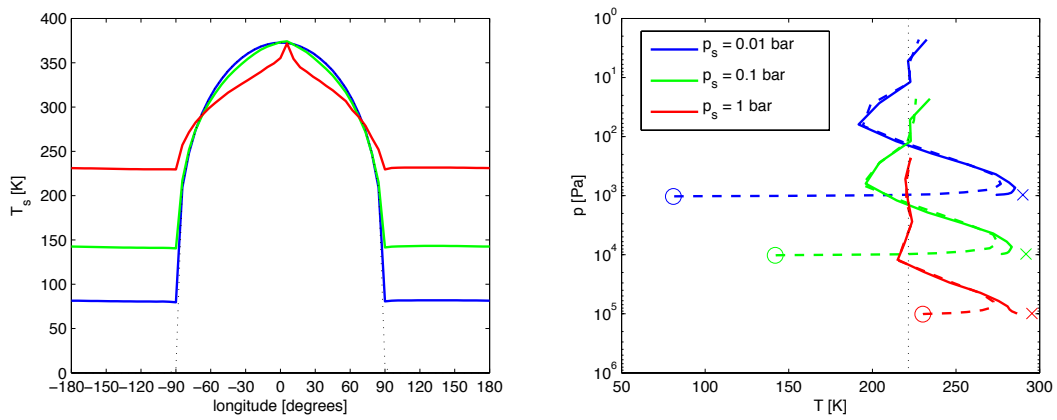


Fig. 2. (left) Temperature profile in the atmosphere. (right) Pressure-temperature profile in the atmosphere. The dashed vertical line indicates the condensation temperature. The solid lines represent the surface temperature profiles for different surface pressures. The dashed lines represent the condensation temperature profiles for different surface pressures.

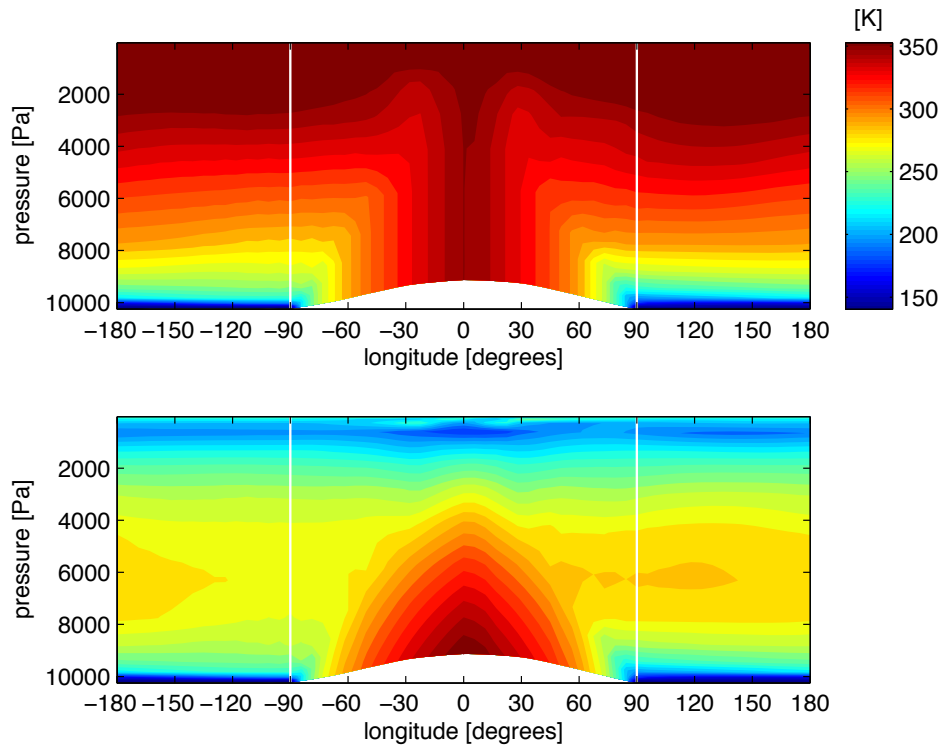


Fig. 3. Temperature profiles of equatorial (a) and equatorial (b) in 0.1 bargay gas in Wh et al. (2014) in the secondary globe

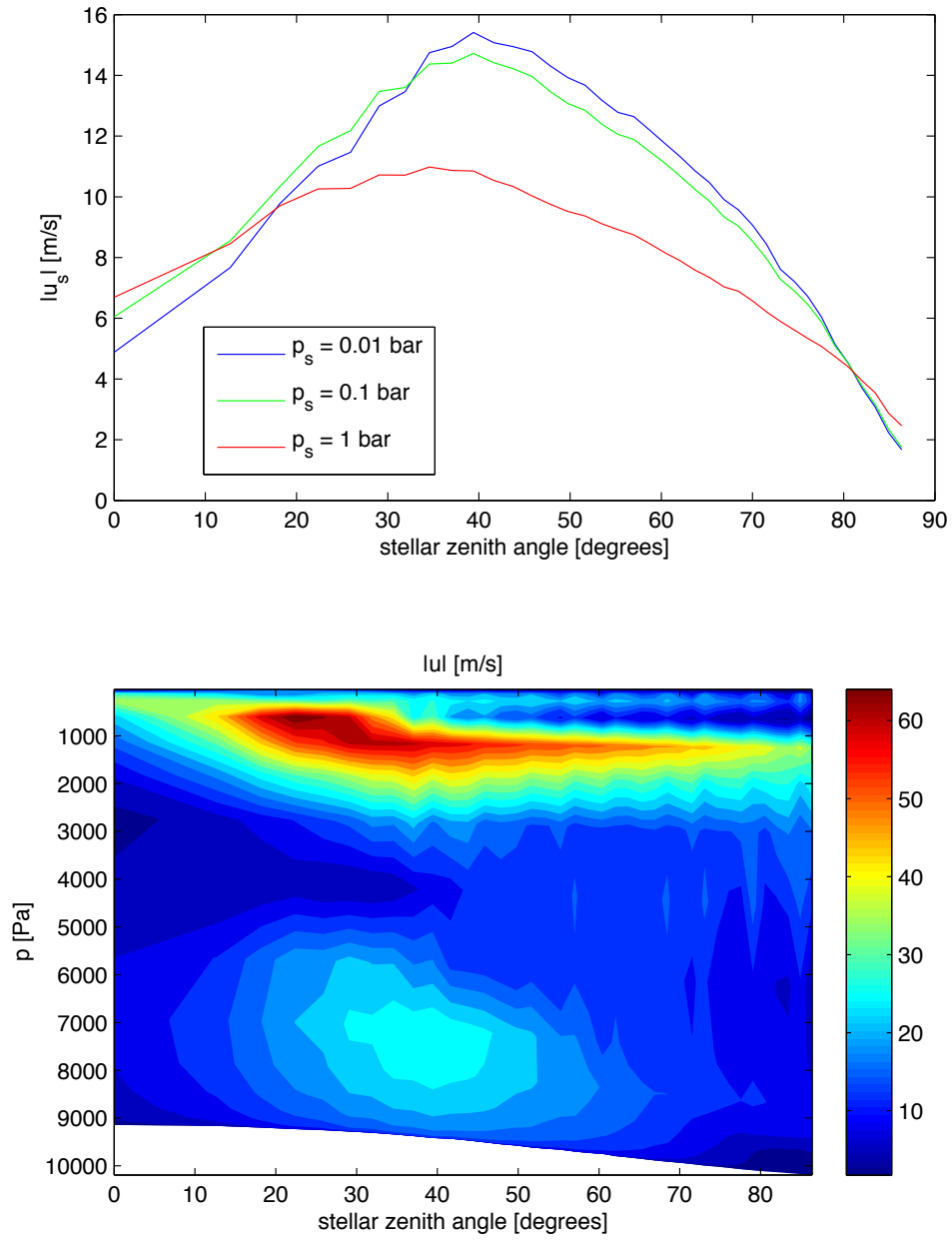


Fig. 5.-(a) Mean surface wind speed change in gaseous
(b) Mean surface wind speed change and p_s in 0.1 bar
gaseous

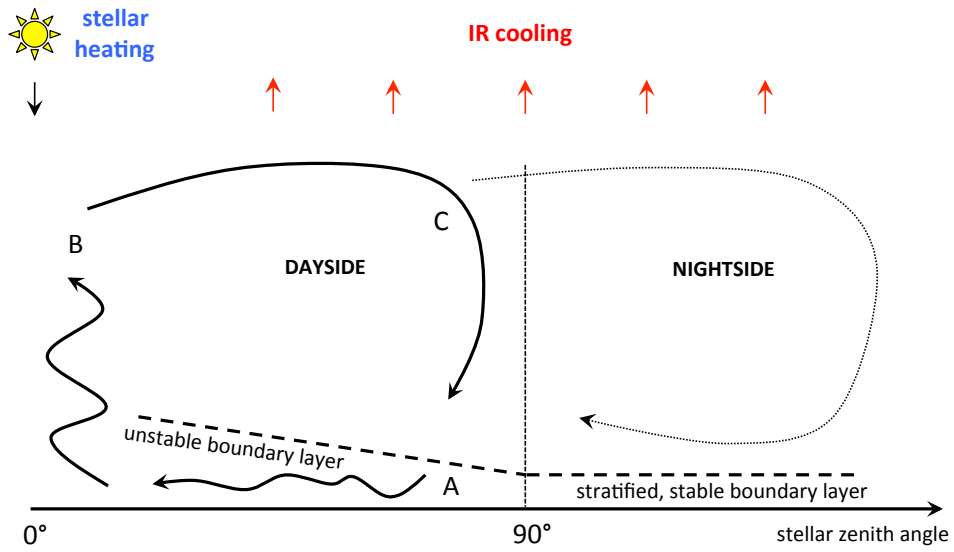


Fig. 6. Schematic of a circulant boundary layer on a planet's surface.

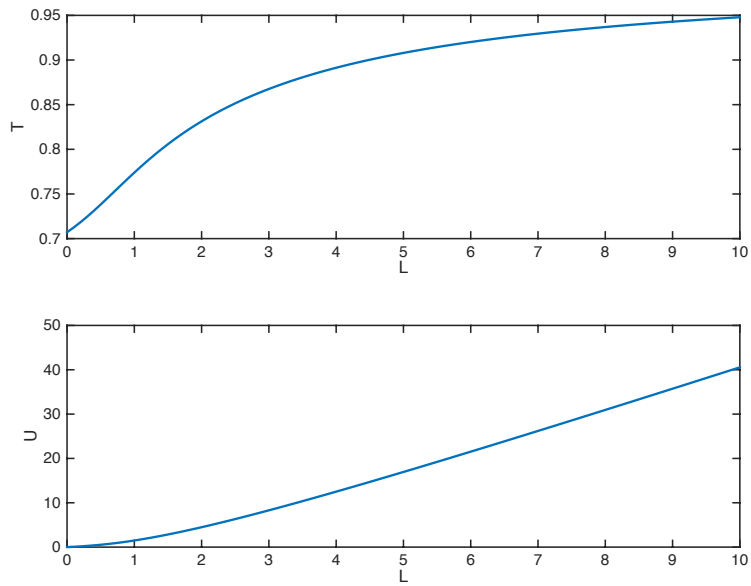


Fig. 7. Profiles of temperature \tilde{T} (a) and velocity \tilde{U} (b) as a function of distance \tilde{L} .

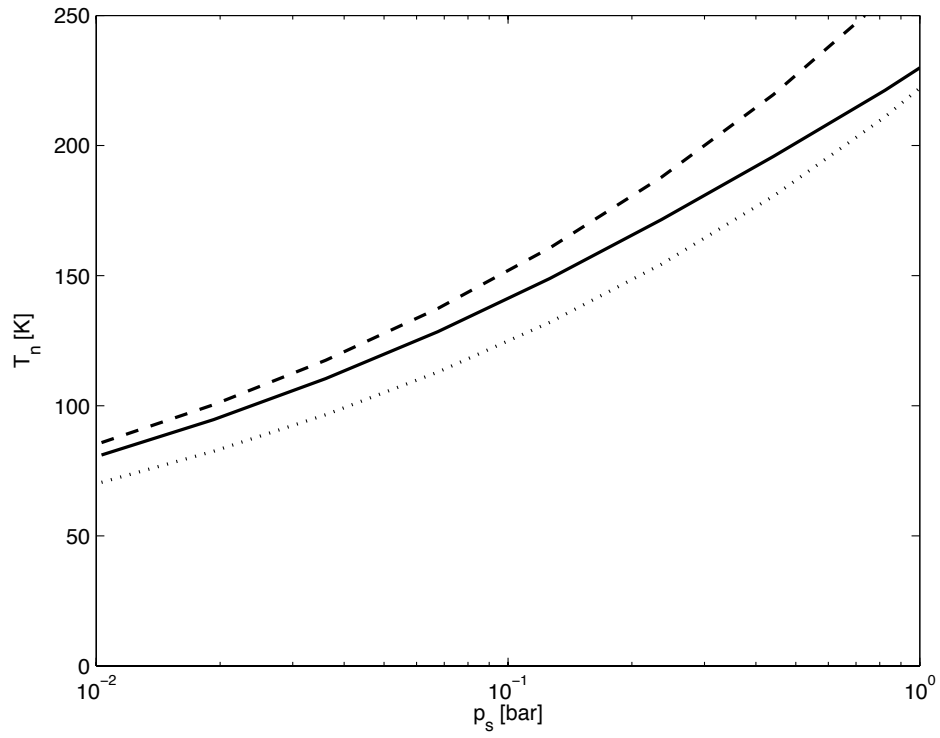


Fig. 8. Mean temperature as a function of surface pressure in a GCM (solid line), predicted by radiative transfer (dotted line) and predicted by radiative + convective transfer (dashed line).

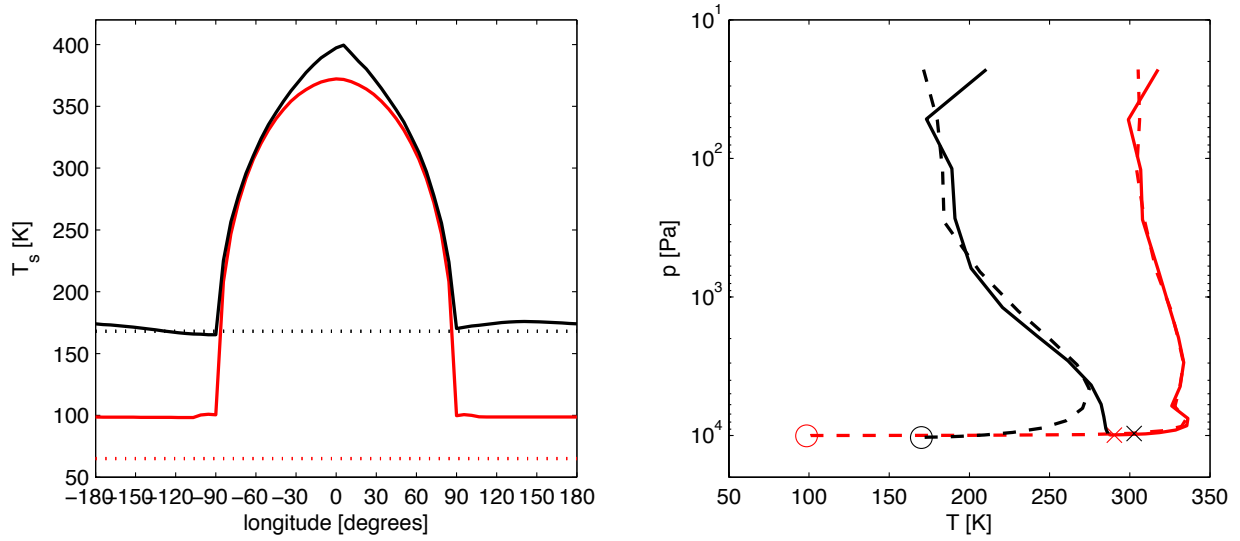


Fig. 9. (left) Time-averaged equifacial temperature profiles at $z=0$ in a
 cold- k CO_2 (black) and CO (red). The dots indicate the
 density at 0.1 bar for each case. (right) Phase diagrams for
 CO_2 (black) and CO (red) showing the phase boundaries
 and the density of the gas phase at 0.1 bar (dots).

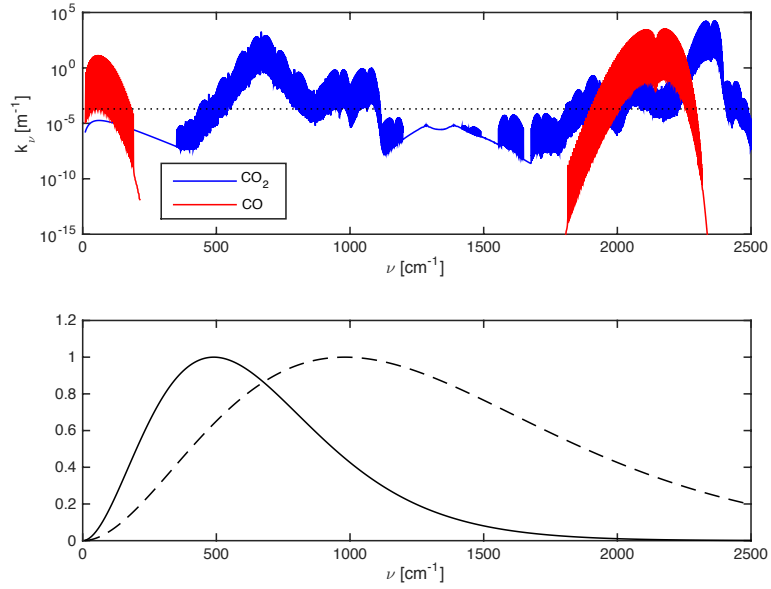


Fig. 10. (a) Infrared absorption coefficient k_ν of CO and CO₂ at 400 K and 0.1 bar. The back
indicates $\tau = Hk_\nu = 1$ for $H = 5$ km. CO₂ and CO are indicated
from top to bottom. (b) Normalized profiles of k_ν at 250 K (solid
line) and 500 K (dashed line).

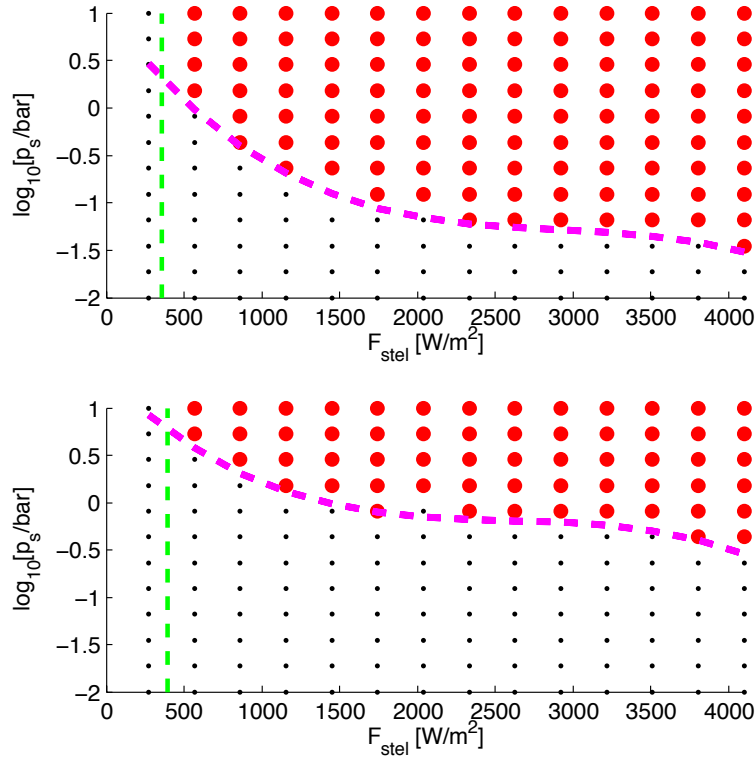


Fig. 11. Stability diagram for CO₂ in a 1 M_{\odot} (a) and a 10 M_{\odot} (b) star. The dashed green line indicates the location of the K-I CO₂ instability. The dashed magenta curve indicates the location of the CO₂ instability. The red dots indicate the region of stability. The black dots indicate the region of instability.